ICAS 2016
30th Congress of the International Council of the Aeronautical Sciences
DCC, Daejeon, Korea ; September 25-30, 2016

PLASTIC DEFORMATION OF POWDER METALLURGY TUNGSTEN ALLOY FOILS FOR SATELLITE ENCLOSURES

M. Kanerva*, E. Sarlin, A. Hållbro***, J. Jokinen***
***Aalto University, Department of Mechanical Engineering, Finland**
****Tampere University of Technology, Department of Materials Science, Finland**
*****Plansee SE, Sweden**

Keywords: *spacecraft, tungsten heavy alloy, hybrid laminate, finite element analysis*

Abstract

Radiation shielding is one of the most crucial features of enclosure materials in spacecraft. The attenuation of electron radiation in hybrid materials, which consist mainly of carbon-fiber-reinforced plastics (CFRP), can be improved by laminating thin tungsten foils between the CFRP layers. In this paper, we study tensile behavior of thin foils to understand the plastic deformation of pure tungsten (W) foils and sintered tungsten heavy alloy (WHA) foils. The performed tests are simulated using the finite element (FE) method. Full 3-D FE models of tungsten and CFRP hybrids are generated to study the non-linearity response of different tungsten material models.

1 Introduction

Varied instrumentation and electronics in satellites are sensitive to proton and electron radiation from the surrounding space environment. For typical structural composites, carbon-fiber-reinforced plastics (CFRPs), the attenuation of electron radiation needs to be improved by laminating thin foils of refractory metal between the composite layers [1, 2]. However, this type of hybrid concepts are prone to delamination due to high residual stresses induced during manufacture and mechanically weak metal-polymer interfaces [3, 4]. Powder metallurgy is a solution to manufacture tungsten-based foils. Sintered tungsten heavy alloy (WHA) foils tend to have lower Young's modulus and also could be more favorable to adhesion-promoting surface treatments [5, 6] when compared to traditional cold-rolled pure tungsten (W) foils in hybrid laminate applications.

In this paper, we study the plastic deformation of W foils and as-sintered WHA foils (thickness from 50 µm to 100 µm). Elastic constants, yielding and ultimate behavior are determined experimentally. The fracture mode in different specimens is studied using scanning electron microscopy. In the second part of the study, the performed tests are simulated using the finite element method. Full 3-D models are generated to study the behavior of 3-D deformable solid elements. Plastic deformation in the foils is modeled using two different plasticity models and three different representations of the models. Finally, the simulated stress-strain curves are compared to the experimental data. The effect of element type and mesh fineness are considered. Based on the results, residual stresses in tungsten-CFRP hybrids are studied.

2 Materials and Methods

2.1 Tungsten Foils

Two tungsten-based foils were studied. First, rolled W foil with a nominal thickness of 50 µm (99.95% purity, Alfa Aesar GmbH, Germany)

was considered as a reference material. Second, specialized WHA alloy (DENSIMET® 176, W-Ni-Fe, Plansee SE, Austria) was studied as a rival. The nominal thickness of the as-sintered WHA foil was 100 µm.

2.2 CFRP Laminates

Pre-preg tape consisting of MTM 57 epoxy resin (Advanced Composites Group, UK) and unidirectional (UD) M40J(12K) carbon fibers (Toray, USA) was obtained from Advanced Composites Group (Umeco, UK). The nominal thickness of the pre-preg was 0.29 mm and its resin content was 32% (weight/weight) meaning an areal weight of 300 g/sqm. The pre-preg tape was used to prepare CFRP laminates for tensile testing. Four different laminates were prepared. Laminate lay-ups of $[0^{\circ}]$, $[0^{\circ}_5]$, $[90^{\circ}_{22}]$ and $[\pm 45^{\circ}_6]_{SE}$ were used for testing mechanical properties in the fiber direction, transverse direction and in shear, respectively. The laminates were vacuum-bagged onto an aluminum mould and cured using an autoclave. A layer of polyamide peel ply was placed between the pre-preg stacks and the vacuum bag. A cure sequence recommended by the manufacturer was used: The sequence included a linear heating ramp (≈1.1 °C/min), 60-minute dwell time, and a constant, 0.8 bar vacuum pressure during the sequence (vacuum was released after the mould temperature finally cooled down to 90 °C).

2.3 Tensile Testing

2.3.1 Tungsten Tensile Testing

Dog-bone-shaped test specimens were cut of the W and WHA foils according to the geometry shown in Fig. 1. Tabs were used at the test machine gripping area in order to prevent the thin foils to fail due to gripping. The tabs were cut of glass-fiber-reinforced epoxy laminate and glued using DP190 (3M, USA) epoxy adhesive. All tests were performed using a universal testing machine with computerized data acquisition and control (Elite Suite, MTS, USA) at a displacement rate of 1.0 mm/min and at ambient laboratory conditions (23.2 °C, 24.4% RH). Strains were measured using stacked rosette (0/90°) strain gauges (KFG-5-120-D16, Kyowa Electronic Instruments, Japan). Strain gauge data was synchronously recorded (Signasoft 6000, Peekel Instruments, NL) with the testing machine. Young's modulus values were determined over the linear strain range ($\Delta\varepsilon$ = 0.2% for pure W and $\Delta\varepsilon$ = 0.1% for WHA) using least-squares-fitting and calculated based on the specimen cross-section at the strain gauge location. Ultimate stress values were based on the exact cross-section at the failure point.

2.3.2 CFRP Tensile Testing

The testing of the CFRP properties in the fiber direction and transverse direction were performed according to the standard ISO 527; different specimen thicknesses were tested to adjust failure load. The testing of in-plane shear modulus was performed according to the standard ASTM D 3518. The tests and specimens are defined in Fig. 1 and Table 1. The test specimen tabs were cut of glass-fiber-reinforced epoxy laminate ($\pm 45^{\circ}$ lay-up) and glued using DP190 (3M) epoxy adhesive. All tests were performed using a universal testing machine with computerized data acquisition and control (Elite Suite, MTS, USA) at a displacement rate of 1.0 mm/min and at ambient laboratory conditions (25.2 °C, 28.9% RH). Strains were measured using uniaxial and stacked rosette (0/90°) gauges (KFG-10-120-D16/C1, Kyowa Electronic Instruments, Japan). An extensometer with a 50 mm gauge length (MTS, USA) was used for comparisons. Strain gauge data was synchronously recorded (Signasoft 6000, Peekel Instruments, NL) with the testing machine. Young's modulus was determined over a linear strain range of $\Delta\varepsilon$ = 0.3% using least-squares-fitting and based on the cross-section at the strain gauge location.

2.4 Scanning Electron Microscopy (SEM)

Fracture surfaces of the tungsten specimens after testing were imaged using a scanning electron microscope; model ULTRAplus (Zeiss, Germany) was used. The samples were cut out of the W and WHA specimens and imaged directly without further sample treatments or coatings.

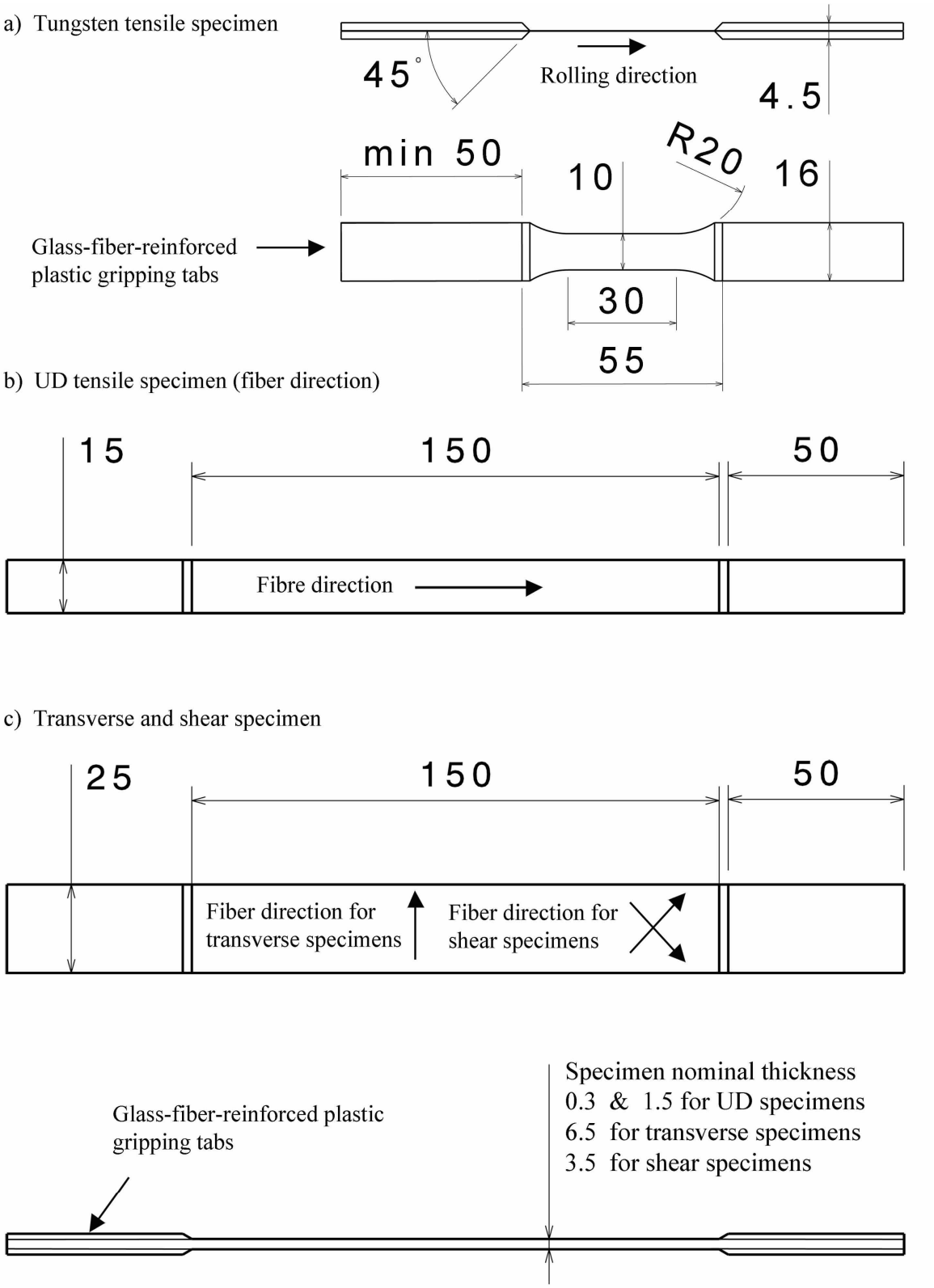

Fig. 1. Test specimen geometries for: (a) tungsten-based specimens; (b) CFRP tensile specimens, and; (c) CFRP tensile transverse and shear specimens. Dimensions are given in millimeters.

Table 1. Test type, applied standards and specimen number per material considered in this study.

Test type	Test standard	Test series	Material
Tensile	-	5	Pure tungsten, thickness 50 µm
Tensile	-	5	WHA alloy foil, thickness 100 µm
Tensile	ISO 527-1…5 (2009)	3	CFRP, lay-up $[0^{\circ}_1]$
Tensile	ISO 527-1…5 (2009)	5	CFRP, lay-up $[0^{\circ}_5]$
Tensile	ASTM D 3039 – 00 (2006)	5	CFRP, lay-up $[90^{\circ}_{22}]$
Shear	ASTM D 3518 – 94 (2007)	5	CFRP, lay-up $[\pm 45^{\circ}_6]_{SE}$

2.5 Finite Element Analysis (FEA)

The simulation work included two different simulation studies. First, the tensile testing of the WHA foil was simulated. Second, a hybrid W-CFRP specimen and its residual stresses due to manufacture were simulated. The modeling and simulations were performed by using a commercial FEA code *Abaqus* 6.14-2 (standard).

2.5.1 Tungsten Tensile Test Simulation

The tensile specimen model was generated using the CAD-model used in the test specimen preparation. For the simulation, the other end of the specimen model was held at initial position by boundary conditions while the other was displaced by applying enforced (uniaxial) displacement to the nodes of the tab surfaces. The applied force was calculated based on the reaction force recorded over the tab surfaces.

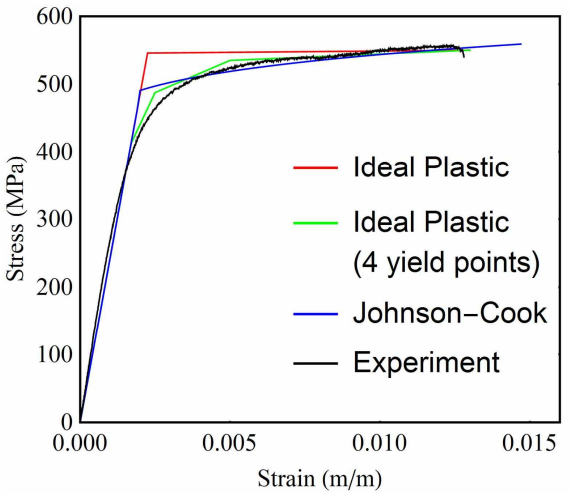

Fig. 2. The three material models applied for the tungsten tensile testing simulation.

Table 2. Parameters of the material models applied for tungsten tensile testing simulation.

Model	Parameters
Ideal Plastic (single yield)	Yield stress = 545.85 MPa
Ideal Plastic (4 yield points)	Yield stress I = 412.42 MPa Yield stress II = 487.5 MPa Plastic strain II = 0.0004905 Yield stress III = 535 MPa Plastic strain III = 0.002795 Yield stress IV = 550 MPa Plastic strain IV = 0.010733
Johnson-Cook $A + B \cdot \varepsilon_p^n$	A = 350.314 MPa B = 483.434 MPa n = 0.199

Two different Abaqus-implemented material models were considered in the simulation of the WHA tensile behavior: Ideal plastic and Johnson-Cook (J-C). For the ideal plastic model, two different alternatives were considered: a model with a single yield point and a model with four-point yielding. The parameters of the models were fitted based on the experimental stress-strain curves, as shown in Fig. 2. The fitted parameters of the models are shown in Table 2. The (linear) elastic constants were input based on the results of the tensile testing (later shown in Table 3). Linear full-integration hexahedrons (C3D8 & C3D8I) were studied as element options. The specimen tabs were meshed using linear C3D4 tetrahedrons. Two levels of mesh fineness were studied to account for possible element shape effects (9222 and 44907 elements in total). A scalar strain comparable to the experimentally measured strain gauge data was established as an average of axial (element centroid) strains

along the real strain gauge grid position (5.0 mm grid length). The model and the two mesh alternatives are shown in Fig. 3. All the simulations were run at double precision using 8 GB of memory (RAM) and a single core from an Intel Xeon 3.2 GHz processor (CPU).

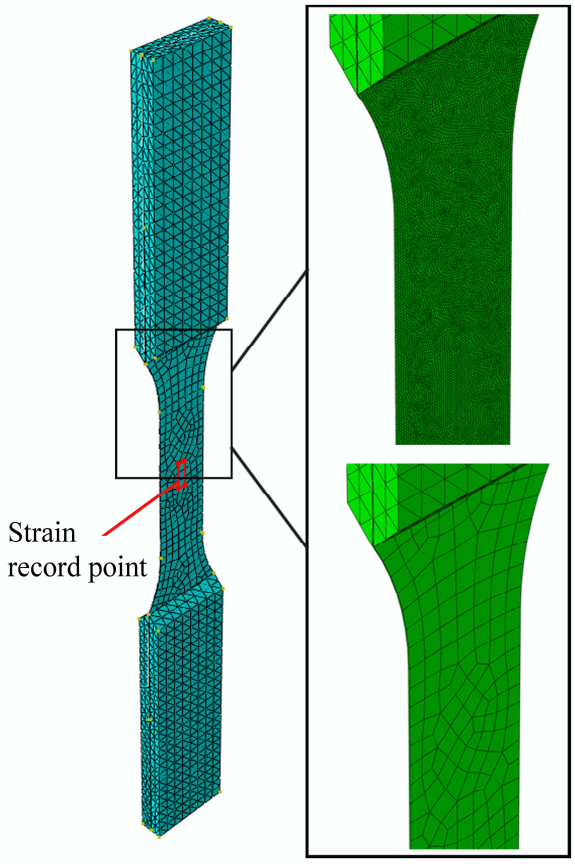

Fig. 3. The test specimen model generated for the FEA of W-Ni-Fe alloy plastic deformation; two alternative mesh fineness levels are shown on the right.

2.5.2 W-CFRP Residual Stress Simulation

A W-CFRP laminate specimen according to our previous study [3] was modeled to estimate the effect of yielding of the metal (tungsten-based) layer due to residual stresses. For simulation, a temperature difference of ΔT = -100 °C was applied over the entire geometry. To prevent the free-body motion, an element set at the other short end of the specimen was held in its initial position by using boundary conditions for three neighboring nodes.

The specimen geometry in the thickness direction was divided into a WHA foil layer and two CFRP parts using partitioning. The J-C material model, fitted based on the tensile testing, was applied to the WHA foil. For the CFRP parts, a linear behavior was presumed using engineering constants with the determined elastic constants (later shown in Table 4). A coefficient of (linear) thermal expansion (CTE) of 4.5 µm/(m°C) [7] was set for the tungsten-based foils. For the CFRP parts, CTEs of -0.43 µm/(m°C) and 44.0 µm/(m°C) [3] were set for the fiber direction and transverse direction, respectively. Instance seed value of 0.2 mm was applied for the WHA foil. For the CFRP layers, an ideal ratio was applied (1:1:1). Von Mises stresses and plastic strains were monitored on the foil surfaces.

3 Results

3.1 Tungsten Foil Tensile Behavior

The determined properties of the tungsten (alloy) foils are shown in Tables 3 and 4 and the stress-strain curves are shown in Figs. 4 and 5. The tensile behavior of the W foils was merely linear up to the failure (≈0.7% average strain). The testing resulted in relatively high scatter of ultimate strain (and stress) values. The failure often occurred at the end of the gauge section of the specimen (shoulder region) and the strain measured by the strain gauge in the center of the gauge section might not have been representative of the actual failure strain leading to scatter in the values. The scatter might also indicate inhomogeneous material – perhaps due to the very high rolling state of the foil. Contrary to the pure tungsten foils, the tensile behavior of the WHA specimens was highly non-linear. A brief linear portion was clearly observable in the beginning (non-linearity point at ≈0.1% strain). The linear portion was followed by a portion of extensive plastic deformation – up to 1.14% strain in average. All the determined tensile properties of the WHA alloy were highly consistent referring to homogenous material in the length scale of the test specimens.

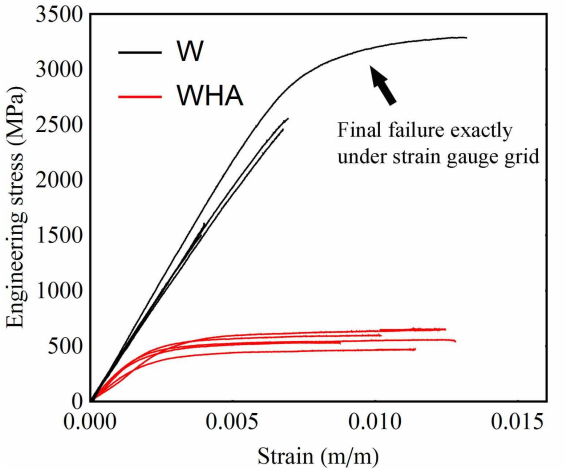

Fig. 4. Experimentally determined stress-strain curves for the pure tungsten and WHA foils.

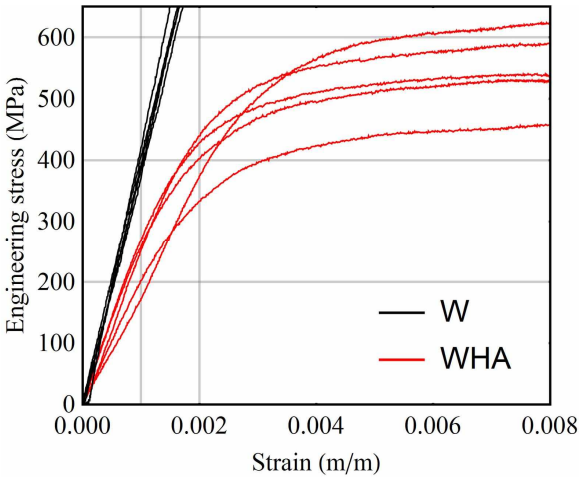

Fig. 5. Magnification to the low-strain region of the stress-strain curves for the W and as-sintered WHA foil.

3.2 Tungsten Foil Fracture Surfaces

The SEM images of the fracture surfaces are shown in Fig. 6. The fracture surface of W evidenced that the rolling of the foil resulted in a layered structure consisting of elongated tungsten grains. No (lateral) necking at the failure point was visually observed from the specimens. In turn, the fracture surface of the WHA specimen revealed large globular shaped W grains (10…40 µm) embedded tightly in Ni-Fe matrix. The matrix seemed to have enabled the ductile behavior up to the point of bulk failure based on the shredding observed on the fracture surface of Ni-Fe matrix. Also, adhesion between the W grains and the Ni-Fe matrix seemed to have been strong – no de-adhesion had progressed into the interfaces between the W grains and Ni-Fe matrix. Quite surprisingly, the WHA specimen's failure point did not show observable necking by visual observation indicating that the plastic deformation occurred evenly throughout the specimen volume between the test machine grips.

a)

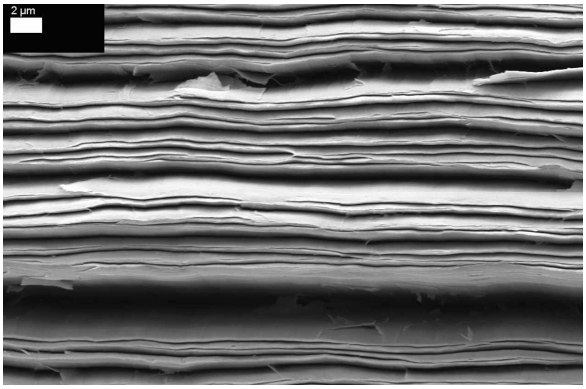

b)

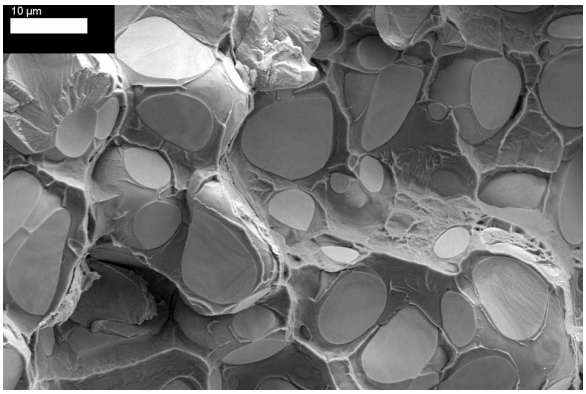

Fig. 6. Fracture surfaces of tungsten specimens after testing: (a) W; (b) as-sintered WHA. Note different scale bars.

3.3 CFRP In-Plane Behavior

The determined properties of the CFRP are shown in Table 5. The determined values were typical of comparable CFRP laminates. The Young's modulus and ultimate strain (and strength) of CFRP were higher when only a single pre-preg layer was tested, i.e. lay-up [0°]. This behavior was presumed to originate from a slightly higher fiber content when excess resin

Table 3. Experimentally determined tensile properties of the W foil (50 μm thickness).

Property	Symbol	Average ± standard deviation	Units	Test series (specimens)
Young's modulus	E	394.4 ± 16	GPa	5
Tensile strength	σ_u	2238 ± 723	MPa	
Ultimate strain	ε_u	0.0070 ± 0.004	m/m	
Poisson's ratio	ν	0.36 ± 0.07	–	

Table 4. Experimentally determined tensile properties of the WHA foil (100 μm thickness).

Property	Symbol	Average ± standard deviation	Units	Test series (specimens)
Young's modulus	E	242.6 ± 48	GPa	5
Non-linearity point	ε_{NL}	0.00099 ± 0.00016	–	
0.2% yield stress	$\sigma_{0.2}$	566.1 ± 26	MPa	
Tensile strength	σ_u	662 ± 27	MPa	
Ultimate strain	ε_u	0.011 ± 0.002	m/m	
Poisson's ratio	ν	0.34 ± 0.05	–	

Table 5. Experimentally determined tensile properties of the CFRP used in this study.

Property	Symbol	Average ± standard deviation	Units	Lay-up	Test series (specimens)
Young's modulus in fiber direction	E_{11}	204.1 ± 12	GPa	$[0^\circ_1]$	3
Tensile strength in fiber direction	$\sigma_{u,11}$	1830 ± 85	MPa	$[0^\circ_1]$	
Ultimate strain in fiber direction	$\varepsilon_{u,11}$	0.0083 ± 0.0003	m/m	$[0^\circ_1]$	
Young's modulus in fiber direction	E_{11}	191.5 ± 7	GPa	$[0^\circ_5]$	5
Tensile strength in fiber direction	$\sigma_{u,11}$	1701 ± 204	MPa	$[0^\circ_5]$	
In-plane Poisson's ratio	ν_{12}	0.305 ± 0.007	–	$[0^\circ_5]$	
Ultimate strain in fiber direction	$\varepsilon_{u,11}$	0.008 ± 0.0009	m/m	$[0^\circ_5]$	
Young's modulus in transverse direction	E_{22}	6.3 ± 0.4	GPa	$[90^\circ_{22}]$	5
Tensile strength in transverse direction	$\sigma_{u,22}$	29.3 *	MPa	$[90^\circ_{22}]$	
Ultimate strain in transverse direction	$\varepsilon_{u,22}$	0.0047 *	m/m	$[90^\circ_{22}]$	
In-plane shear modulus	G_{12}	7.2 ± 0.3	GPa	$[\pm 45^\circ_6]_{SE}$	5

* Value based on the specimen with final failure in the centre of the specimen gauge section.

Fig. 7. Typical failure modes for the CFRP test specimens: (a) UD specimen; (b) shear specimen.

better flowed into the peel ply cloth during cure and also due to lower micro-flaw probability of the thin specimens. Typical failure modes of the specimens are shown in Fig. 7, where it can be seen that the tensile, unidirectionally reinforced specimens shattered in the fiber direction prior to the final fiber breakage. For the shear specimens, the failure was gradual and the specimens did not break into two parts until a very high shear beyond 6% strain. For the transverse direction specimens, $[90^{\circ}_{22}]$, the failure occurred mostly at the test specimen gripping area and, therefore, the ultimate values are estimated based on one test specimen only.

3.4 Accuracy of the WHA Models

The simulated stress-strain curves using the coarse element mesh and the three different material models are shown in Fig. 8. It can be seen that all the models perform the target load and strain (≈1%) well despite the non-fit element shape (1:1:0.07) in the coarse mesh. The result of the single yield Ideal Plastic model at the yield point region was poor, expectedly.

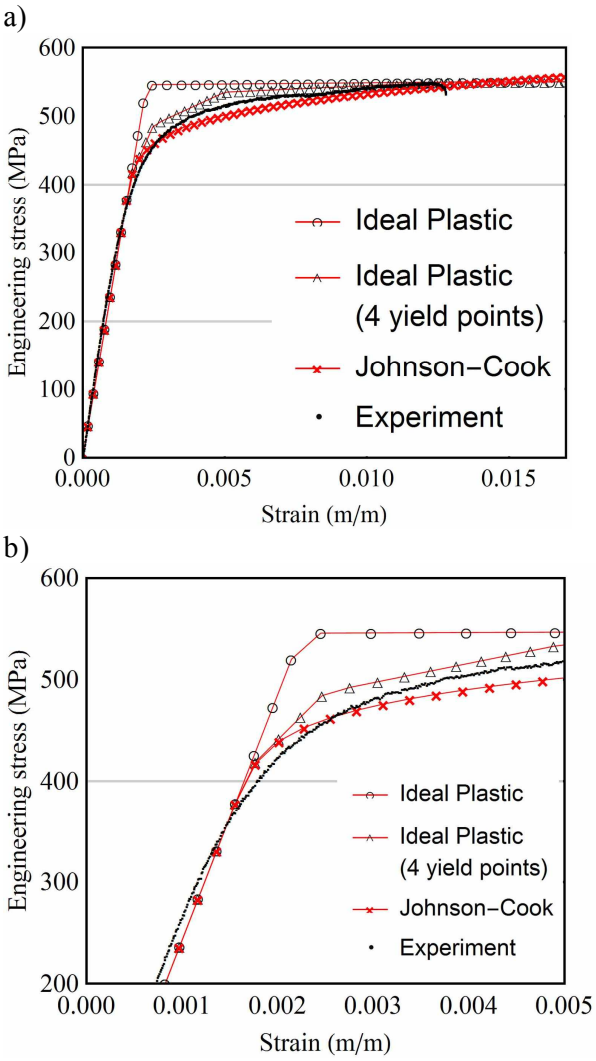

Fig. 8. Simulated stress-strain curves for the WHA foil: (a) overall behavior; (b) magnification to the yield region. A coarse element mesh was used for all cases.

3.5 Mesh-Dependency of the Models

The stress-strain curves simulated using the fine element mesh and the Johnson-Cook material model are shown in Fig. 9. It is clear that the mesh fineness did not have an effect on the performance of the simulation. Moreover, the element type did not have an effect on the simulated plastic deformation – at least for the tensile loaded specimen model studied here.

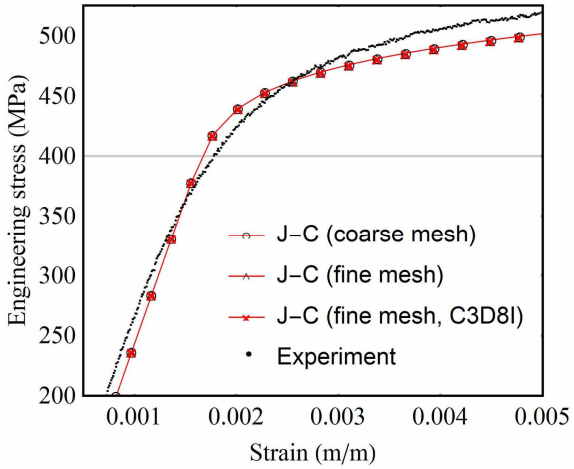

Fig. 9. Simulated stress-strain curves for the WHA foil around the yield region. A fine element mesh was used for all cases.

3.6 Computational Efficiency of the Models

The total CPU time required per material model is shown in Figs. 10(a)-(b). The J-C model resulted in a ≈35% saving in the computational time compared to the Ideal Plastic models. In turn, the difference between the two Ideal Plastic models was minor. The mesh fineness affected radically the CPU time, and also the difference between the models – the superiority of the J-C model was evidenced by the 53% saving in the computational time. The accounting for the enhanced bending behavior (C3D8I element type) resulted in increased CPU time by approximately 40% (for the J-C model).

3.7 Effects of Plasticity on Residual Stresses

The distributions of von Mises stress (element-wise) on the surface of the simulated W and WHA alloy foils inside the CFRP hybrid are shown in Fig. 11. The comparison between the simulation results for W and WHA suggests that by using a WHA foil the residual stresses due to the elevated temperature-cure of the CFRP pre-preg (at 120 °C, ΔT = -100 °C) decrease 31%.

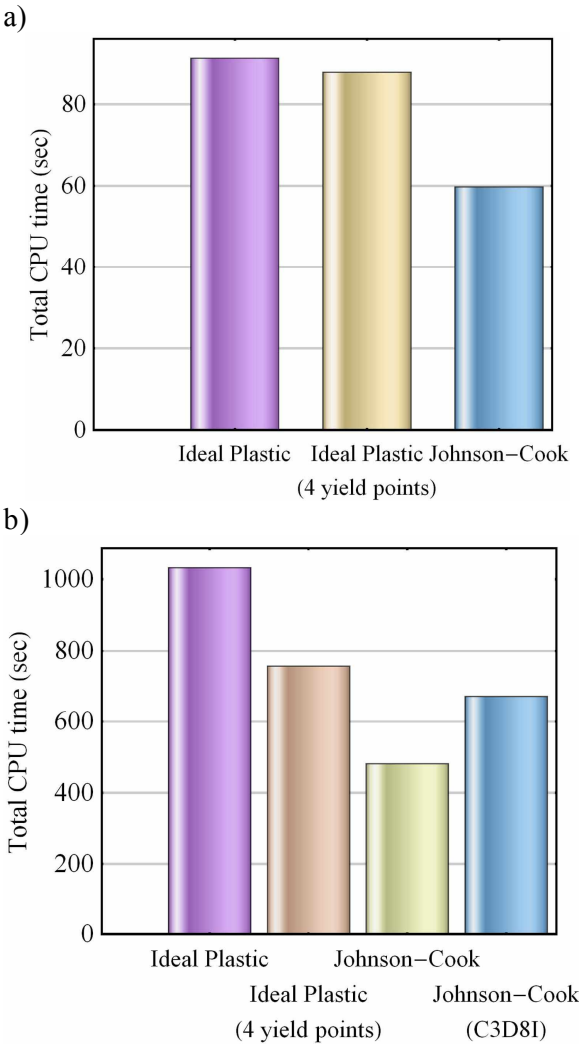

Fig. 10. Total CPU time required per material model: (a) results using a coarse mesh and C3D8 element; (b) results using a fine mesh and two different element types. Incrementation was limited to ≤ 2.5% of the enforced displacement for all cases.

Due to the thermal expansion mismatch in the hybrid, the WHA layer deforms plastically. The magnitude of the plastic strain ('von Mises-effective' scalar, PEMAG) at ΔT = 100 °C reached 0.05% in the central region of the foil. The yielding was mostly due to compressive strain in the specimen transverse (Y) direction.

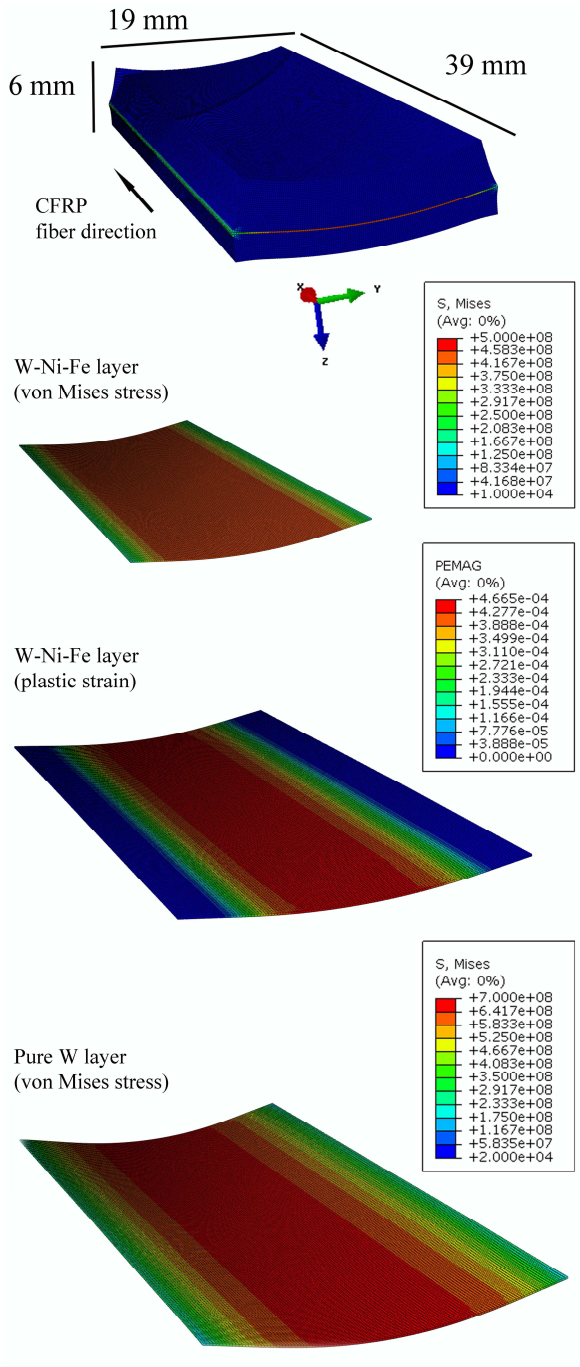

Fig. 11. Simulated residual stresses in a hybrid tungsten-CFRP laminate specimen applying either linear-elastic W layer or plastic deforming as-sintered WHA layer. The thermal load for the simulation was ΔT = -100 °C (simulating the cool-down phase of an autoclave cycle in reality). The deformation scale is ×60.

Respectively, the von Mises stress was around 450 MPa. In other words, the non-linearity point was exceeded but either $\sigma_{0.2}$ level or the stress-strain plateau was not. In comparison, pure W layer efficiently resisted the expansion of the CFRP parts and experienced von Mises stresses as high as ≈660 MPa.

4 Conclusions

In this study, two different tungsten-based foils were investigated. Pure tungsten (W) foil and as-sintered tungsten heavy alloy (WHA) foil were tensile tested and three different material models for the finite element method were developed. The results showed that the WHA foil is capable of plastic deformation up to 1.14% in average and it can be efficiently modeled using a Johnson-Cook strain-hardening model. The simulation of a hybrid laminate consisting of carbon-fiber-reinforced plastic (CFRP) and a tungsten-based foil indicated that the WHA foil is an ideal selection for radiation protection materials from the mechanical integrity point of view. The residual stresses in the WHA-CFRP system were predicted to be 31% lower compared to a system of W-CFRP.

Acknowledgements

The research leading to these results has received funding from the European Community's Seventh Framework Programme (FP7/2007-2013) under Grant Agr. 262746.

References

[1] Mangeret M, Carriere T, Beaucour J. Effects of material and/or structure on shielding of electronic devices. *IEEE Transactions Nuclear and Plasma Sciences*, Vol. 43, No. 6, pp 2665-2670, 1996.

[2] Atxaga G, Marcos J, Jurado M, Carapelle A, Orava R. Radiation shielding of composite space enclosures. *Proc 63rd International Astronautical Congress*, held in Naples, (Italy), C2, pp 1-10, 2012.

[3] Kanerva M, Jokinen J, Antunes P, Wallin M, Brander T, Saarela O. Acceptance testing of tungsten-CFRP laminate interfaces for satellite enclosures. *Proc 20th International Conference on Composite Materials*, held in Copenhagen (Denmark), P101-5, pp 1-12, 2015.

[4] Kanerva M, Jokinen J, Sarlin E, Saarela O. Apparent fracture toughness versus micro-scale fracture toughness of interfaces – The challenge of critical values. *ASTM Materials Performance and Characterization*, Vol. 3, SPECIAL ISSUE, pp 173-188, 2014.

[5] Kanerva M, Koerselman JR, Revitzer H, Johansson L-S, Sarlin E, Rautiainen A, Brander T, Saarela O. Structural assessment of tungsten-epoxy bonding in spacecraft composite enclosures with enhanced radiation protection. *Proc European Conference on Spacecraft Structures, Materials, and Environmental Testing*, held in Braunschweig (Germany), ESA SP-727, pp 1-6, 2014.

[6] Kanerva M, Johansson L-S, Campbell JM, Revitzer H, Sarlin E, Brander T, Saarela O. Hydrofluoric–nitric–sulphuric-acid surface treatment of tungsten for carbon fiber-reinforced composite hybrids in space applications. *Applied Surface Science*, Vol. 328, No. 1, pp 418-427, 2015.

[7] Zhang X, Yan Q, Yan C, Wang T, Ge C. Microstructure, mechanical properties and bonding characteristic of deformed tungsten. *International Journal of Refractory Metals and Hard Materials*, Vol. 43, No. 1, pp 302-308, 2014.

Contact Author Email Address

mailto: mikko.kanerva@aalto.fi

Copyright Statement

The authors confirm that they, and/or their company or organization, hold copyright on all of the original material included in this paper. The authors also confirm that they have obtained permission, from the copyright holder of any third party material included in this paper, to publish it as part of their paper. The authors confirm that they give permission, or have obtained permission from the copyright holder of this paper, for the publication and distribution of this paper as part of the ICAS 2016 proceedings or as individual off-prints from the proceedings.